


Fluctuation-frustrated flat band instabilities in NdNiO₂

Mi-Young Choi,¹ Warren E. Pickett^{2,*} and Kwan-Woo Lee^{1,3,†}

¹Department of Applied Physics, Graduate School, Korea University, Sejong 30019, Korea

²Department of Physics, University of California Davis, Davis, California 95616, USA

³Division of Display and Semiconductor Physics, Korea University, Sejong 30019, Korea

 (Received 6 May 2020; revised 15 July 2020; accepted 25 August 2020; published 18 September 2020)

The discovery that Nd_{1-x}Sr_xNiO₂, with the CaCuO₂ infinite-layer structure, superconducts up to 15 K around the hole-doping level $x = 0.2$ raises the crucial question of its fundamental electronic and magnetic processes. The unexplained basic feature that we address is that, for $x = 0$ and as opposed to strongly antiferromagnetic (AFM) CaCuO₂, NdNiO₂ with the same structure and formal d^9 configuration does not undergo AFM order. We study this issue not in the conventional manner, as energetically unfavored or as frustrated magnetic order, but as an instability of the AFM phase itself. We are able to obtain the static AFM ordered state, but find that a flat band, one-dimensional-like van Hove singularity (vHs) is pinned to the Fermi level. This situation is unusual in a non-half-filled, effectively two-band system. The vHs makes the AFM phase unstable to spin-density disproportionation, breathing, and half-breathing lattice distortions, and (innate or parasitic) charge-density disproportionation. These flat band instabilities, distant relatives of single-band cuprate models, thereby inhibit but do not eliminate incipient AFM tendencies at low temperature. The primary feature is that a pair of active bands ($d_{x^2-y^2}$, d_{z^2}) eliminate half-filled physics and, due to instabilities, preclude the AFM phase seen in CaCuO₂. This strongly AFM correlated, conducting spin-liquid phase with strong participation of the Ni d_{z^2} orbital forms the platform for superconductivity in NdNiO₂.

DOI: [10.1103/PhysRevResearch.2.033445](https://doi.org/10.1103/PhysRevResearch.2.033445)

I. INTRODUCTION

A disparate variety of interacting models [1–14] based on density functional theory (DFT) studies [15–22] have been proposed to illuminate the electronic and magnetic behavior underlying the discovery [23] and experimental study [24–26] of long-sought superconductivity in a layered nickelate, specifically hole-doped NdNiO₂ (NNO). With the same infinite-layer structure as CaCuO₂ (CCO), which superconducts up to 110 K when doped [27], NNO displays several differences with CCO. Undoped NNO is conducting; CCO is insulating; CCO orders antiferromagnetically, whereas no signature of order is seen in NNO (and its isoelectronic but nonsuperconducting sister LaNiO₂ (LNO) [28–31]) and there is no sign of heavy-fermion screening of Ni moments. CCO and NNO have a common d^9 (formal) configuration (one hole) on the transition metal ion, however, NNO persists as (poorly) conducting to low temperature. Central differences include positioning of metal $3d$ levels relative to O $2p$ levels that are substantially different in the two compounds [18], the presence of Nd $5d$ character at the Fermi level [16,17], and the interesting effects of Nd $4f$ character in the magnetic system [17].

The electronic structures of the d^9 infinite-layer cuprates and nickelates were compared some time ago, with some similarities but substantial differences being noted [15,16] and quantified more recently by Wannier function analysis [18,19], and some impact of the Nd moments has been noted [17]. The similarities but substantial difference continue to dominate the discussion and inform the models cited above. No items, however, seem as fundamental as the difference in ground states of the undoped materials: antiferromagnetic (AFM) insulator for CCO, and disordered moment conductor for NNO, the latter being a conducting quantum paramagnetic (MQPM) phase in the Sachdev-Read classification [32]. Based on an interacting two-band model, Werner and Hoshino [5] discussed NNO in terms of the spin-freezing theory of unconventional superconductivity [33,34], and the potentially simpler case of superconductivity at high pressure in elemental Eu with disordered f^7 moments [35] might share in this behavior.

Here, we focus on this absence of (AFM) ordering of Ni moments in NNO, moments whose ordering has been the overriding hallmark of the undoped phase in cuprates. In closely related layered nickelates [36–40] (viz., La₃Ni₂O₆, La₄Ni₃O₈, La₄Ni₃O₁₀) even with nonintegral formal Ni valences magnetic ordering and sometimes charge ordering occur; none has a ground state without symmetry breaking, unlike NNO. The conventional means of addressing the appearance of magnetic order is as an instability of the nonmagnetic metallic state, either via Stoner or Ruderman-Kittel-Kasuya-Yosida (RKKY) instabilities as indicated by the static susceptibility $\chi(\vec{q})$ or as instability to insulating character with interatomic exchange constants. Leonov *et al.*

*wepickett@ucdavis.edu

†mckwan@korea.ac.kr

Published by the American Physical Society under the terms of the [Creative Commons Attribution 4.0 International license](https://creativecommons.org/licenses/by/4.0/). Further distribution of this work must maintain attribution to the author(s) and the published article's title, journal citation, and DOI.

provide an example of the conventional approach [2] applied to NNO (actually LaNiO_2) and extended to the DFT + DMFT (dynamical mean field theory).

In spite of being energetically favored in the absence of fluctuations (i.e., in DFT calculations [16–18]) and evaluations of near-neighbor exchange coupling in the 10–18 meV (120–200 K) range [2,12,21], the AFM ordered state is not observed, suggesting it is a metastable but physically inaccessible phase. The AFM state of NNO is, however, accessible computationally, allowing study of its electronic structure and microscopic processes that *render AFM order unstable*, thereby giving insight into the inaccessibility of the AFM phase.

We should note that the questions we address lie exactly in the broad controversy in this field: Is this nickelate basically similar to the infinite-layer cuprates, or essentially different? The similarities have been emphasized by, for example, Botana and Norman, who obtain significant but not defining differences in some of the electronic characteristics of LaNiO_2 and CaCuO_2 , and also offer that doping tends to make them even more similar [18]. Jiang and collaborators contend that the underlying Ni ion (and its environment) is essentially different from the cuprates, being at its core nonmagnetic, and they offer therefore that the pairing mechanism must be basically different from the cuprates [12]. Lechermann reaches related conclusions [7], but there are stimulating results on both sides of this question. Our work expands on our earlier study [16] and tends to accentuate differences from the cuprates, rather than similarities.

Our methods are described in Sec. II, followed by a brief discussion of relative energies and magnetic moments in Sec. III. Section IV provides a description of the (experimentally inaccessible) AFM ordered state, pointing out the effects of electronic correlation due to the onsite repulsion U . The Fermi surfaces of this AFM state, and their change with low levels of doping, are described in Sec. V. Sections VI and VII give a description of the magnetic (and charge) and lattice instabilities, respectively, that arise. A short wrapup of our work is presented in Sec. VIII.

II. OVERVIEW OF METHODS

To treat the strong intra-atomic Coulomb interactions on Nd and Ni ions, we adopt the generalized gradient approximation [41] plus fully anisotropic Coulomb U (GGA + U) method [42], as implemented in the accurate all-electron full-potential code WIEN2K [43]. As described in our previous work [17], this approach retains the all-electron character of Nd which provides intra-atomic Nd $d-f$ exchange coupling but is not the subject here. With the lattice parameters experimentally observed for the superconducting thin films of $\text{Nd}_{0.8}\text{Sr}_{0.2}\text{NiO}_2$ [23], a $\sqrt{2} \times \sqrt{2}$ supercell is used to investigate the AFM state, where both Ni and Nd layers have antialigned moments. In the supercell the frozen O full-breathing motion is investigated, whereas the half-breathing motion is calculated in a 2×2 supercell (see below). In the infinite-layer structure, the Nd ion lies above/below the NiO_2 square by $c/2 = 1.685 \text{ \AA}$, the Ni-O distance is 1.96 \AA . Description of lattice displacements is described as they are encountered in the paper.

For purposes of comparison, we provide comparisons of crystal structures and ionic sizes of NdNiO_2 and CaCuO_2 . For NNO, $a = 3.92 \text{ \AA}$, $c = 3.37 \text{ \AA}$ [23]; for CCO, $a = 3.86 \text{ \AA}$, $c = 3.20 \text{ \AA}$ [44], with cell volumes 51.8 and 47.7 \AA^3 , respectively, an 8% difference. The relevant Shannon-Prewitt ionic radii are Nd^{3+} : 1.25 \AA , Ca^{2+} : 1.12 \AA . Square planar Cu^{2+} is 0.55 \AA ; unfortunately, Ni^{1+} is so rare that no value is agreed, but extrapolating from other formal valences a reasonable guess is 10%–15% larger. These differences account for the smaller volume CCO. Of importance for NNO is k_z dispersion of the d_{z^2} bands, which is larger in NNO due to hopping through the Nd $5d$ orbitals in spite of the larger interlayer separation in NNO. The effects of the different Madelung potentials, lowering of the O $2p$ bands in NNO, have been discussed in several of the papers cited in Sec. I.

In the GGA + U calculations, for the Nd ions, the Hubbard $U_f^{\text{Nd}} = 8.0 \text{ eV}$ and the Hund's exchange coupling $J_f^{\text{Nd}} = 1.0 \text{ eV}$ are fixed in all calculations, which provide the $S = \frac{3}{2} \text{ Nd}^{3+}$ spin state [17]. The total angular momentum $\mathcal{J} = \frac{9}{2}$ gives a correspondingly large total magnetic moment. We varied U_d^{Ni} in the range of 0–5 eV, to study correlation effects up to the value that is reasonable for Ni ions in a conducting oxide, and with fixed $J_d^{\text{Ni}} = 0.7 \text{ eV}$. We quote values of U_d^{Ni} (simply called U) that we explore. As discussed in following sections, including U on Ni is essential but the electronic structure near the Fermi level is practically invariant to U in the 2–5 eV range. We have mostly focused on results for $U = 4 \text{ eV}$.

In WIEN2K, the basis size was determined by $R_{mt} K_{\text{max}} = 8$ and the augmented-plane-wave radii R_{mt} of Nd 2.50, Ni 1.95, and O 1.65, in atomic units. The other input parameters of these calculations are the same as in our previous study of NdNiO_2 [17].

III. ENERGIES AND MOMENTS

The (110) AFM state we study, within a $\sqrt{2} \times \sqrt{2}$ supercell, has both antialigned Nd and Ni spin layers, with the structure giving no net near-neighbor Nd-Ni coupling. This AFM ordering is energetically favored over aligned Ni spins by 95 (62) meV/f.u. at $U = 0$ (4) eV, both being strongly favored over nonmagnetic Ni [17,18]. A theoretical value of the energy for local but disordered Ni moments requires separate calculations, but at maximum would be of the order of J_d^{Ni} . Leonov *et al.*, for example, obtain first- and second- neighbor exchange constants that put it in the regime of magnetic frustration within the J_1 - J_2 spin model only upon electron doping [2]. Although DFT often overestimates magnetic moments and thereby energies in weak magnets, it is commonly accurate for larger (ionic) moments. These Ni moments are of the order of $1\mu_B$. Adding the effect of U revises the energetics and increases the moments somewhat, but not the relative stabilities of AMF and FM order. The observed avoidance by NNO of a relatively large ordering energy is our focus.

IV. CORRELATION EFFECTS AND THE FLAT BAND

Correlation effects are immediate and unexpected. One thing that proceeds as expected is that the Ni $d_{x^2-y^2}$ bands are split by the order of U ; in cuprates this opens a gap. In the nearest-neighbor tight-binding picture these bands are

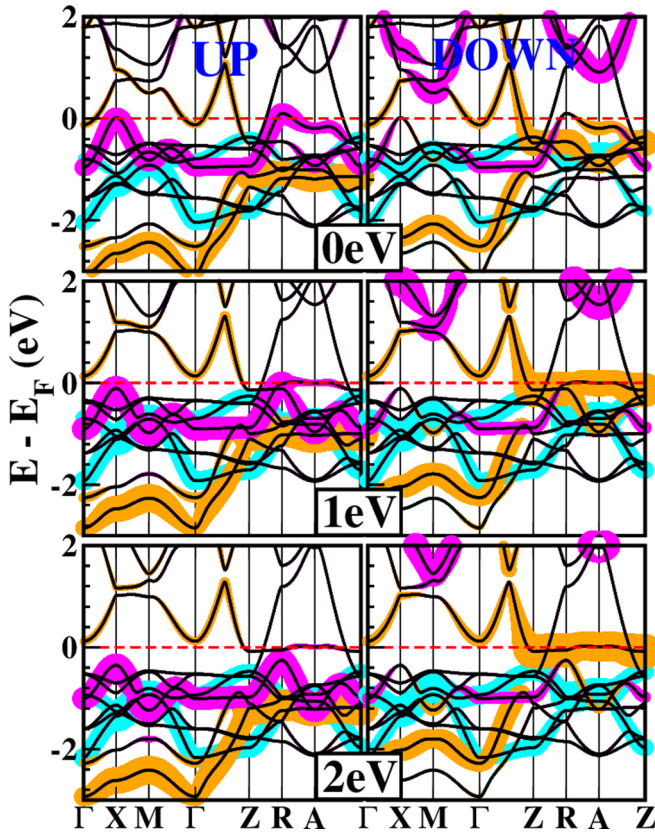


FIG. 1. Fatband depiction of the AFM band structure in GGA + U , $U = 0, 1, 2$ eV: (left) Ni majority; (right) Ni minority; $E_F \equiv 0$. Characters that are emphasized are Ni d_{z^2} (orange), $d_{x^2-y^2}$ (magenta), and d_{xy} (blue), relative to the primitive cell. The d_{z^2} band flattens along the Z - R - A - Z lines ($k_z = \pi/c$ zone face) already for $U = 1$ eV. Relative to the primitive cell, symmetry points are rotated by 45° in the $\sqrt{2} \times \sqrt{2}$ AFM supercell, i.e., $M(R) \leftrightarrow X(A)$.

perfectly nested in the diamond-shaped region that becomes the Brillouin zone (BZ) in the AFM zone. From either a perfect nesting perspective or a superexchange spin model, a gap is opened and AFM order is robust.

However, including even a small value of U leads to a dramatic change in the Ni d_{z^2} -derived band initially below but very near the Fermi energy E_F . This band shows k_z dispersion assisted by the Nd d orbital, but negligible dispersion for $k_z = \pi/c$ (Z - R - A - Z lines), where the bands remain degenerate in spite of being half-filled.

Figure 1 shows in fatband form the Ni d_{z^2} (orange), $d_{x^2-y^2}$ (magenta), and d_{xy} (blue) band characters as U increases over the range 0–2 eV; d_{xz} , d_{yz} orbitals of both spin are occupied. At $U = 0$, all three orbitals are active near E_F . However, already with the modest value $U = 1$ eV, an unanticipated flatness of the d_{z^2} band emerges precisely at E_F along the entire top zone face $k_z = \pi/c$ while some (but small) dispersion remains in the $k_z = 0$ plane. This distinctive flat band remains in place as U increases to 5 eV, not shown in the figure. To emphasize: the flat band on the upper/lower zone face is a robust feature of AFM order and two-band behavior, with implications discussed below.

The relatively short Ni-Ni distance 1.685 Å along the c axis induces a hopping (assisted by Nd d_{z^2} and d_{xy}) between the

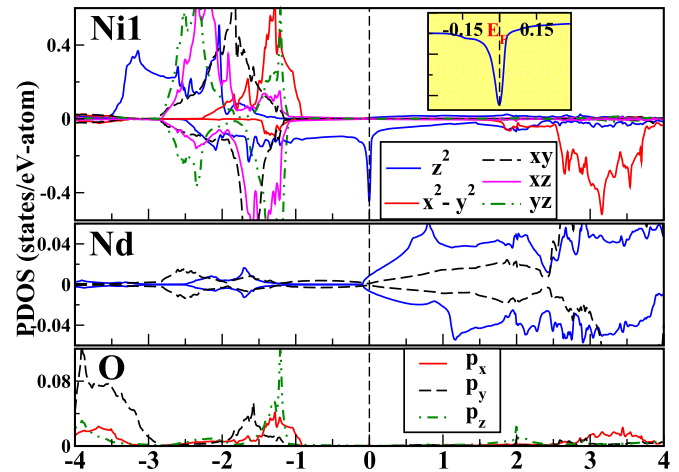


FIG. 2. AFM orbital-projected densities of states (PDOSs)/atom of Ni $3d$, two Nd $5d$ d_{z^2} and d_{xy} orbitals, and O $2p$ orbitals, for the undistorted lattice at $U = 4$ eV, in the $3d$ band region (note the difference in scales). Majority (minority) are plotted upward (downward). The oxygen PDOS lies below 3 eV. Having E_F pinned precisely at the sharp, 1D-like vHs (upper panel, minority spin, shown enlarged in the inset) produces the instabilities discussed in the text.

d_{z^2} orbitals on nearby layers, leading to dispersion of 2 eV along the Γ - Z line. For NNO, the related effective hopping parameter is $t_{d_{z^2}} \approx 1$ eV, large for k_z hopping across a 3.4-Å distance but aided by the Nd $5d$ orbital. For the minority (higher-energy) states, the Ni d_{z^2} orbital is mixed with Nd d_{xy} and somewhat with Nd $d_{x^2-y^2}$ on the $k_z = \pi/c$ plane, resulting in a hybridization gap of 0.4 eV at the Z point. The mixtures elsewhere, viz., at Γ , are negligible.

Figure 2 shows (for the realistic metallic value $U = 4$ eV) Ni, Nd, and O orbital-projected densities of states (PDOSs) in the d band region surrounding E_F . The unfilled minority Ni $d_{x^2-y^2}$ orbital (the hole) lies at +3 eV. One remarkable feature is that the minority Ni d_{z^2} band spans nearly 5 eV, crossing E_F and ensuring a conducting state. All other Ni d orbitals of both spins are narrow. The other notable feature is that this same orbital gives rise to a flat band across the entire $k_z = \pi/c$ zone face that produces a one-dimensional (1D) van Hove singularity (vHs) pinned at E_F , with pure d_{z^2} character; recall, these two exotic features are robust, that is, insensitive to U . The valence bands have nearly pure Ni d_{z^2} character within 1 eV of E_F . Nd $5d$ character extends down to and slightly below E_F as noted several times previously, but does not participate in the flat band. Around Z (see along the Z - R and Z - A lines in Fig. 1), the flat band crosses a dispersive band with mixed Nd $5d_{z^2}$, Ni $3d_{xz/yz}$ character at E_F .

As a result of coupling through Nd states, the flat band acquires a small width ~ 40 meV corresponding to an effective *in-plane* hopping $t_{z^2}^{\text{eff}} = 20$ meV for this plane. Based on charge decompositions and PDOSs, and the Ni d_{z^2} character above E_F , the evidence suggests a formal valence closer to $\text{Ni}^{1.4+}$ rather than Ni^{1+} as would be appropriate for an insulator. (Since O is clearly 2−, we expect this is a breakdown of formal valence counting as often occurs in metals.) In contrast to cuprates where the central role implicates the Cu $d_{x^2-y^2}$ orbital, our results support previous indications [16] that the

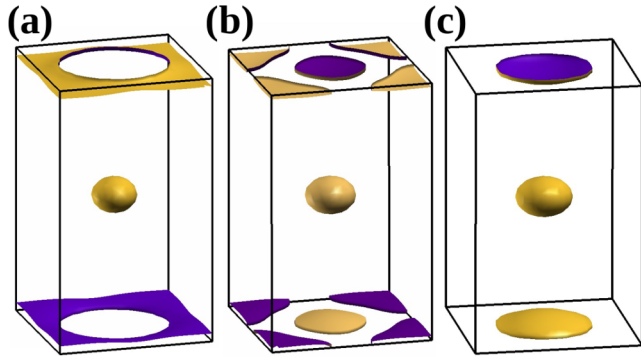


FIG. 3. Variations of AFM Fermi surfaces by carrier dopings: (a) 0.025 hole doping, (b) undoped, and (c) 0.025 electron doping per f.u. at $U = 4.0$ eV. Small doping levels (virtual crystal) were chosen to probe the geometry of the (nearly) flat band.

Ni d_{z^2} orbital becomes a central player in NNO (and LNO), with the $d_{x^2-y^2}$ hole being more of a given and less of a dynamical component.

V. FERMI SURFACES VERSUS DOPING

To probe the geometry of the (nearly) flat band, the AFM Fermi surfaces (FSs) for $U = 4$ eV versus small (virtual crystal) doping levels are shown in Fig. 3. A Γ -centered electron sphere, a mixture of Ni $3d_{z^2}$ and Nd $5d_{z^2}$ characters [16,17], arises from the high velocity band and slowly changes volume upon doping. 2D wafers appear near the $k_z = \pm\pi/c$ planes. At stoichiometry, a round hole wafer is centered at Z and a rounded-diamond electron wafer at the zone corner A . For hole doping, the thin hole wafer is pinched off around the Z point [Fig. 3(a)], and the electron wafers connect. In small electron doping [Fig. 3(c)], only electron buttons appear around Z .

The flat and thin wafer and button FSs at stoichiometry have a characteristic thickness $2K_z^F \leq 0.06\frac{\pi}{c}$. In addition to the flatness, the very small velocities will lead to strong nesting, at K_z^F and $\frac{2\pi}{c} - 2K_z^F$. The related susceptibility will encourage spin density, charge density, and lattice fluctuations, and possibly instabilities at $\sim 32c$ and $\sim 2c$, respectively. The long-wavelength instability would be challenging to study numerically, the short-wavelength one corresponds to a dimerization of successive NiO_2 layers, a Peierls instability of the d_{z^2} band and its associated vHs peak.

VI. MAGNETIC INSTABILITY

A flat band generated DOS peak at E_F in an AFM metal causes a possible “meta-Stoner” instability of the AFM order (Stoner instability being with respect to the already spin-polarized state). To break the underlying spin symmetry in this already magnetically ordered AFM state, the spin symmetry must be broken. We have studied this magnetic instability together with lattice instability by imposing breathing and half-breathing types of oxygen distortions [see Fig. 4(a)], which destroy the equivalence of the Ni ions. For the former, the unit cell is not enlarged; for the latter, the cell is doubled, with Ni ions of each spin direction being squeezed, or not,

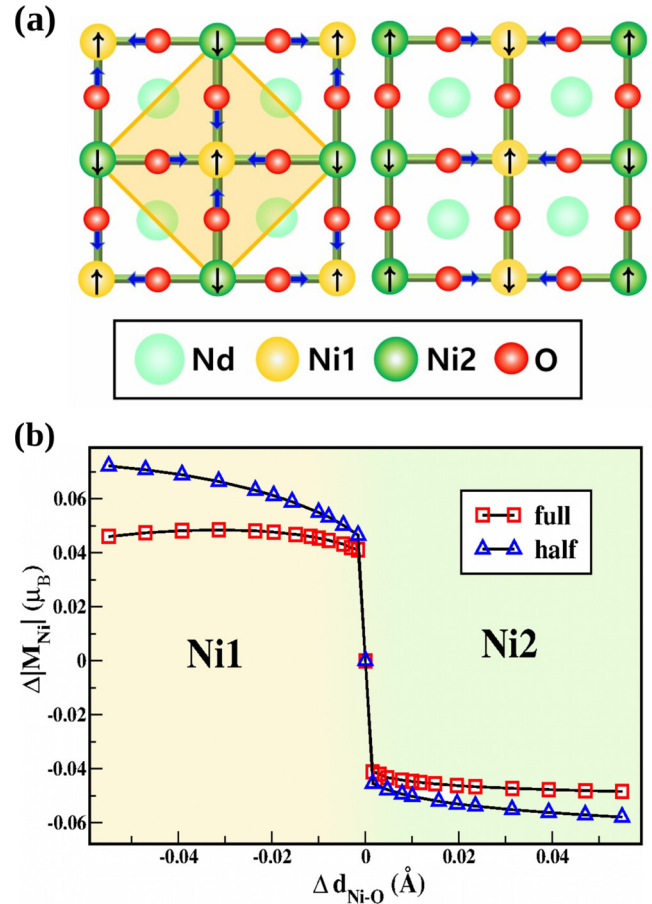


FIG. 4. (a) Sketch of of the NiO_2 layer with (left) oxygen full-breathing mode and (right) half-breathing mode along (100) direction, showing 2×2 primitive cells. The full- and half-breathing modes allow for checkerboard and stripe charge and spin orders, respectively. The arrows on the Ni ions indicate spins of Ni ions, whereas the blue (thick) arrows denote the displacement of oxygen ions. (b) Changes of the magnitude of Ni magnetic moments ΔM , versus changes in the Ni-O bond length $\Delta d_{\text{Ni-O}}$ for both the full- and half-breathing modes at $U = 4$ eV. This “spin disproportionation” instability occurs for the undistorted lattice. There is an accompanying charge disproportionation (see text).

by the half-breathing distortion. The range of displacements is shown in Fig. 4(b).

For the full- and half-breathing modes, the changes in moments of the two Ni sites, Ni1 and Ni2, are displayed in Fig. 4(b). These frozen oxygen phonon modes lead to an unexpected change in the Ni magnet moments even for a very small displacement, indicating the magnetic instability is there even for the symmetric lattice. Tiny mode amplitudes (displacements down to 0.001 \AA extrapolating to zero; allowing for symmetry breaking is what is important) produce a “spin disproportionation” of the AFM ions of the order of $\pm 0.05\mu_B$. This behavior signals that the AFM state is unstable to a first-order transition to a ferrimagnetic state, which reflects the partially itinerant character of the Ni moments. The mechanism is the vHs generated meta-Stoner instability, with feedback within the self-consistency loop (necessitated by the vHs) providing the first-order nature; actual lattice

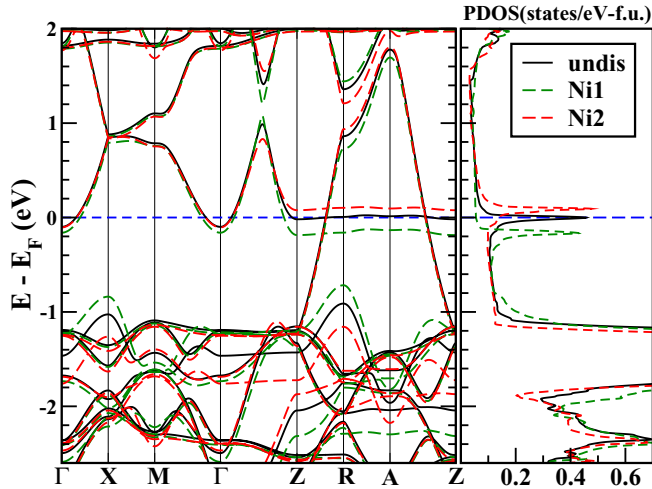


FIG. 5. AFM band structures and Ni atom PDOSs for $U = 4$ eV. The (red and green) dashed lines indicate the bands split by the full-breathing mode, with O displaced by 0.03 Å. The energy splitting of each band per unit displacement is 5 eV/Å. The half-breathing mode (not shown) shows similar band splitting. The peak splitting is the source of the Peierls (meta-Stoner) charge (spin) instability.

distortion is unnecessary. The magnetic symmetry breaking is accompanied by a Ni1-to-Ni2 charge disproportionation up to $\sim \pm 0.05e$ (from atomic sphere charges). Being accompanied by the charge disproportionation as well, these results suggest there would be substantial magnetic and charge fluctuations in the AFM state, contributing to its evident instability.

VII. LATTICE INSTABILITY

The effect of the breathing mode on the band structure is displayed in Fig. 5, quantifying the splitting of the vHs peak. The splitting of the peak at E_F due to the frozen phonon modes leads to a characteristic deformation potential (splitting of each band per unit displacement) of $\mathcal{D} = 150$ meV/ 0.03 Å = 5 eV/Å on the $k_z = \pm\pi/c$ planes [45]. This value places AFM NNO in the strong electron-phonon coupling regime. Due to the vHs giving strong structure in the density of states $N(E)$, this splitting of the vHs peak varies in the range of 3.1 to 7.3 eV/Å for displacements in the range 0.01 to 0.047 Å. This variation leads to strong effects on the electronic and magnetic properties, as discussed below.

To explore the Peierls lattice instability, we plot the energy difference divided by squared amplitude $K(u) = \Delta E(u)/u^2$ in Fig. 6; this is the lattice stiffness (effective force constant) K . For a harmonic phonon $K(u)$ would be a constant, with deviation indicating anharmonicity. The energy change with oxygen displacement u , $\Delta E(u) = E(u) - E(0)$, can be fit very well by $A_2u^2 + A_3u^3$. The obtained coefficients are $A_2 = 47.5$ eV/Å², $A_3 = 61.2$ eV/Å³ (breathing); $A_2 = 29.4$ eV/Å², $A_3 = 136.7$ eV/Å³ (half-breathing). As shown in the inset of Fig. 6, these values are insensitive to the strength of U in the range of 3–5 eV. The harmonic terms provide the frequency of each breathing mode (see below), whereas the A_3u^3 terms quantify anharmonicity.

The calculated $K(u)$ is anomalous in two ways. For typical oxygen vibrational amplitudes 0.05–0.10 Å, it would be

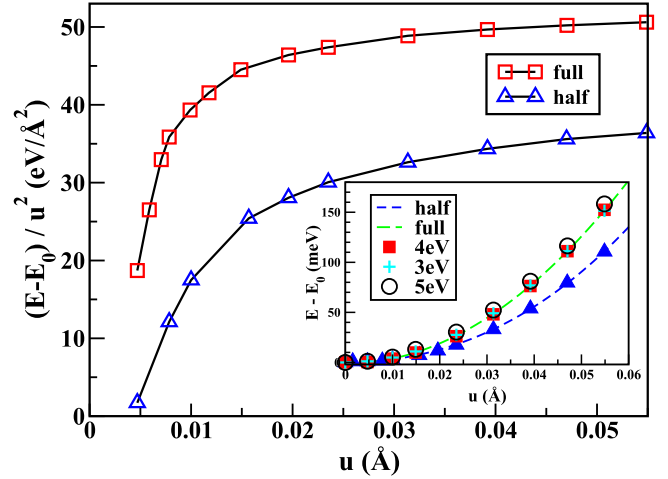


FIG. 6. Energy distortions for the frozen-in oxygen full- and half-breathing modes at $U = 4$ eV. As shown in the inset, these follow a quadratic plus lowest-order anharmonic term, indicated by the green (blue) dashed lines, and are insensitive to strength of U in the range of 3–5 eV.

practically constant; high-frequency O modes typically do not show significant anharmonicity. Figure 6, however, shows that for both breathing and half-breathing modes, $K(u)$ is only beginning to approach a steady value somewhere above 0.05 Å. Second, $K(u)$ drops precipitously below 0.02 Å and extrapolates to *negative* values below 0.005 Å, viz., giving the classic unstable Mexican hat potential surface. Modern linear response lattice dynamics codes that incorporate infinitesimal distortions would calculate imaginary frequencies in both cases, the signature of lattice instabilities for both types of modes. This behavior is revealing the response of the electronic vHs to (infinitesimal) perturbation, analogous to the magnetic instability discussed above.

If calculated as often done on a mesh of u such as 0.01, 0.02, 0.03 Å, etc., the unstable region would not be sampled carefully, but anharmonicity [nonconstancy of $K(u)$] would be evident; high-energy modes around $\omega = 80$ and 60 meV for the full- and half-breathing modes, respectively, would be obtained, similar to our values. Compared with the values for these modes in CaCuO₂ [46] and in La₂CuO₄ [47], these frequencies are smaller by 10%–25%, respectively. Both of these compounds are insulators with no important anharmonicity being reported.

The lattice and magnetic instabilities reflect the sharp and narrow vHs that negates normal charge response and provides a platform that is extremely sensitive to any symmetry breaking that splits the vHs peak. The most anomalous response is confined to small distortions and energies (and thus low temperature), as is clear from Fig. 6. For this Peierls instability, a fully quantum treatment would require self-consistent treatment of (1) anharmonicity, (2) nonadiabatic electron-lattice coupling around the vHs point (where heavy charge carriers are coupled to phonons of similar, or even higher, energy), and (3) behavior of coupled quasiparticle self-energies, which is far beyond the scope of this paper.

A fully quantum treatment would include also the effects of oxygen zero-point fluctuations (ZPFs) on the system and

its response. For frequencies of 60–80 meV, the oxygen zero-point amplitude $\langle u_0 \rangle \approx 0.04\text{--}0.05 \text{ \AA}$. Within this distance of the oxygen site, the potential becomes strongly anharmonic and finally negative. To what extent ZPFs could temper the static lattice, spin, and charge instabilities might be challenging to determine because ZPF effects are subtle: the fully quantum metal has zero resistivity at $T = 0$ because ZPFs do not scatter carriers, whereas the simple picture of averaging over displaced atoms would (incorrectly) suggest otherwise.

An important dynamical lattice consequence for this AFM system is that the vHs will be renormalized at low temperature, narrowed instead of the naive expectation of broadening [48] by electron-phonon interaction, and the issue of the behavior of the nonadiabatic coupled electron-phonon excitations is not settled. Just how the massive flat band carriers would deal with all of these instabilities would be a challenging theoretical problem, but the experimental outcome is that the underlying AFM order we have modeled gives way to a disordered moment metal.

VIII. DISCUSSION: AVOIDANCE OF THE AFM PHASE

We have explored the experimentally inaccessible AFM ordered state of NdNiO₂ with correlated DFT methods. This is the state whose calculated energy indicates it should be the ground state versus nonmagnetic and competing simple magnetic states, and presumably the disordered moment phase as well, seemingly a severe problem for theory. However, we find as well that this state is multiply unstable: lattice, spin, or charge fluctuations, neglected in this static lattice, fixed spin DFT modeling, so further studies would be necessary to progress to a determination and understanding of the ground state. Experiments indicate a conducting state without magnetic order, but likely with fluctuating moments (Ni and Nd) that make it very challenging to model from a DFT viewpoint.

Specifically, we have shown that in the (unphysical) AFM ordered phase a Ni d_{z^2} flat band pinned at the Fermi level arises on the entire $k_z = \pm\pi/c$ zone faces, giving rise to a 1D-like van Hove singularity that supports spin, charge, and lattice (both full- and half-breathing mode) instabilities of the ideal infinite-layer lattice. Due to the narrowness of the vHs, these coupled order parameters may be affected by quantum zero-point oxygen motion and nonadiabatic electron-lattice coupling in the vHs peak, finally frustrating these types of symmetry breaking. These observations account qualitatively for the stabilization of the observed symmetric (conducting, no spin order) phase.

Yet, the AFM ordered state, calculated to be most stable for the static lattice, remains inaccessible by experiment, hence evidently is higher in *free energy* than the conducting spin-disordered state. We propose that as temperature is lowered, NdNiO₂ approaches the AFM ordered phase but encounters its incipient instabilities with strong spin, charge, and lattice fluctuations that inhibit spin order and lattice distortion, thereby stabilizing the symmetric lattice. The result is to remain spin disordered but with AFM correlations, i.e., incipient AFM order, that will reduce the spin free energy. This correlated spin-liquid phase, the Sachdev-Read MQPM phase that has been proposed in another disordered moment superconductor [35], provides the platform for the superconductivity that appears upon hole doping. None of these complications occur in CaCuO₂.

ACKNOWLEDGMENTS

We acknowledge S. Kim for a critical reading of the manuscript. M.Y.C. and K.W.L. were supported by National Research Foundation of Korea Grant No. NRF-2019R1A2C1009588. W.E.P. was supported by NSF Grant No. DMR 1607139.

-
- [1] L.-H. Hu and C. Wu, Two-band model for magnetism and superconductivity in nickelates, *Phys. Rev. Research* **1**, 032046 (2019).
 - [2] I. Leonov, S. L. Skornyakov, and S. Y. Savrasov, Lifshitz transition and frustration of magnetic moments in infinite-layer NdNiO₂ upon hole doping, *Phys. Rev. B* **101**, 241108(R) (2020).
 - [3] S. Ryee, H. Yoon, T. J. Kim, M. Y. Jeong, and M. J. Han, Induced magnetic two-dimensionality by hole doping in the superconducting infinite-layer nickelate Nd_{1-x}Sr_xNiO₂, *Phys. Rev. B* **101**, 064513 (2020).
 - [4] X. Wu, D. D. Sante, T. Schwemmer, W. Hanke, H. Y. Hwang, S. Raghu, and R. Thomale, Robust $d_{x^2-y^2}$ -wave superconductivity of infinite-layer nickelates, *Phys. Rev. B* **101**, 060504(R) (2020).
 - [5] P. Werner and S. Hoshino, Nickelate superconductors: Multi-orbital nature and spin freezing, *Phys. Rev. B* **101**, 041104(R) (2020).
 - [6] G.-M. Zhang, Y.-F. Yang, and F.-C. Zhang, Self-doped Mott insulator for parent compounds of nickelate superconductors, *Phys. Rev. B* **101**, 020501(R) (2020).
 - [7] F. Lechermann, Late transition metal oxides with infinite-layer structure: Nickelates versus cuprates, *Phys. Rev. B* **101**, 081110(R) (2020).
 - [8] H. Zhang, L. Jin, S. Wang, B. Xi, X. Shi, F. Ye, and J.-W. Mei, Effective Hamiltonian for nickelate oxides Nd_{1-x}Sr_xNiO₂, *Phys. Rev. Research* **2**, 013214 (2020).
 - [9] H. Sakakibara, H. Usui, K. Suzuki, T. Kotani, H. Aoki, and K. Kuroki, Model Construction and a Possibility of Cuprate-Like Pairing in a New d^9 Nickelate Superconductor (Nd, Sr)NiO₂, *Phys. Rev. Lett.* **125**, 077003 (2020).
 - [10] Y. Gu, S. Zhu, X. Wang, J. Hu, and H. Chen, A substantial hybridization between correlated Ni-d orbital and itinerant electrons in infinite-layer nickelates, *Commun. Phys.* **3**, 84 (2020).
 - [11] J. Chang, J. Zhao, and Y. Ding, Hund-Heisenberg model in superconducting infinite-layer nickelates, [arXiv:1911.12731](https://arxiv.org/abs/1911.12731).
 - [12] M. Jiang, M. Berciu, and G. A. Sawatzky, Critical Nature of the Ni Spin State in Doped NdNiO₂, *Phys. Rev. Lett.* **124**, 207004 (2020).
 - [13] T. Zhou, Y. Gao, and Z. D. Wang, Spin excitations in nickelate superconductors, *Sci. China-Phys. Mech. Astron.* **63**, 287412 (2020).

- [14] J. Karp, A. S. Botana, M. R. Norman, H. Park, M. Zingl, and A. Millis, Many-body Electronic Structure of NdNiO_2 and CaCuO_2 , *Phys. Rev. X* **10**, 021061 (2020).
- [15] V. I. Anisimov, D. Bukhvalov, and T. M. Rice, Electronic structure of possible nickelate analogs to the cuprates, *Phys. Rev. B* **59**, 7901 (1999).
- [16] K.-W. Lee and W. E. Pickett, Infinite-layer nickelate LaNiO_2 : Ni^{1+} is not Cu^{2+} , *Phys. Rev. B* **70**, 165109 (2004).
- [17] M.-Y. Choi, K.-W. Lee, and W. E. Pickett, Role of 4f states in infinite-layer NdNiO_2 , *Phys. Rev. B* **101**, 020503(R) (2020).
- [18] A. S. Botana and M. R. Norman, Similarities and Differences between LaNiO_2 and CaCuO_2 and Implications for Superconductivity, *Phys. Rev. X* **10**, 011024 (2020).
- [19] Y. Nomura, M. Hirayama, T. Tadano, Y. Yoshimoto, K. Nakamura, and R. Arita, Formation of a two-dimensional single-component correlated electron system and band engineering in the nickelate superconductor NdNiO_2 , *Phys. Rev. B* **100**, 205138 (2019).
- [20] P. Jiang, L. Si, Z. Liao, and Z. Zhong, Electronic structure of rare-earth infinite-layer RNiO_2 ($R = \text{La}, \text{Nd}$), *Phys. Rev. B* **100**, 201106(R) (2019).
- [21] Z. Liu, Z. Ren, W. Zhu, Z. F. Wang, and J. Yang, Electronic and magnetic structure of infinite-layer NdNiO_2 : Trace of antiferromagnetic metal, *npj Quantum Mater.* **5**, 31 (2020).
- [22] B. Geisler and R. Pentcheva, Fundamental difference in the electronic reconstruction of infinite-layer versus perovskite neodymium nickelate films on $\text{SrTiO}_3(001)$, *Phys. Rev. B* **102**, 020502(R) (2020).
- [23] D. Li, K. Lee, B. Y. Wang, M. Osada, S. Crossley, H. R. Lee, Y. Cui, Y. Hikita, and H. Y. Hwang, Superconductivity in an infinite-layer nickelate, *Nature (London)* **572**, 624 (2019).
- [24] M. Hepting, D. Li, C. J. Jia, H. Lu, E. Paris, Y. Tseng, X. Feng, M. Osada, E. Been, Y. Hikita, Y.-D. Chuang, Z. Hussain, K. J. Zhou, A. Nag, M. Garcia-Fernandez, M. Rossi, H. Y. Huang, D. J. Huang, Z. X. Shen, T. Schmitt *et al.*, Electronic structure of the parent compound of superconducting infinite-layer nickelates, *Nat. Mater.* **19**, 381 (2020).
- [25] Q. Li, C. He, J. Si, X. Zhu, Y. Zhang, and H.-H. Wen, Absence of superconductivity in bulk $\text{Nd}_{1-x}\text{Sr}_x\text{NiO}_2$, *Commun. Mater.* **1**, 16 (2020).
- [26] Y. Fu, Y. Fu, A. Wang, H. Cheng, S. Pei, X. Zhou, J. Chen, S. Wang, R. Zhao, W. Jiang, C. Liu, M. Huang, X. Wang, Y. Zhao, D. Yu, F. Ye, S. Wang, and J.-W. Mei, Core-level x-ray photoemission and Raman spectroscopy studies on electronic structures in Mott-Hubbard type nickelate oxide NdNiO_2 , [arXiv:1911.03177](https://arxiv.org/abs/1911.03177).
- [27] M. Azuma, Z. Hiroi, M. Takano, Y. Bando, and Y. Tekeida, Superconductivity at 110 K in the infinite-layer compound $(\text{Sr}_{1-x}\text{Ca}_x)_{1-y}\text{CuO}_2$, *Nature (London)* **356**, 775 (1992).
- [28] M. Crespín, P. Levitz, and L. Gataineau, Reduced forms of LaNiO_3 perovskite. Part 1. Evidence for new phases: $\text{La}_2\text{Ni}_2\text{O}_5$ and LaNiO_2 , *J. Chem. Soc., Faraday Trans. 2* **79**, 1181 (1983).
- [29] M. A. Hayward, M. A. Green, M. J. Rosseinsky, and J. Sloan, Sodium hydride as a powerful reducing agent for topotactic oxide de-intercalation: Synthesis and characterization of the nickel(I) oxide LaNiO_2 , *J. Am. Chem. Soc.* **121**, 8843 (1999).
- [30] D. Kaneko, K. Yamagishi, A. Tsukada, T. Manabe, and M. Naito, Synthesis of infinite-layer LaNiO_2 films by metal organic decomposition, *Physica C (Amsterdam)* **469**, 936 (2009).
- [31] A. Ikeda, T. Manabe, and M. Naito, Improved conductivity of infinite-layer LaNiO_2 thin films by metal organic decomposition, *Physica C (Amsterdam)* **495**, 134 (2013).
- [32] S. Sachdev and N. Read, Metallic spin glasses, *J. Phys.: Condens. Matter* **8**, 9723 (1996).
- [33] S. Hoshino and P. Werner, Superconductivity from Emerging Magnetic Moments, *Phys. Rev. Lett.* **115**, 247001 (2015).
- [34] P. Werner, S. Hoshino, and H. Shinaoka, Spin-freezing perspective on cuprates, *Phys. Rev. B* **94**, 245134 (2016).
- [35] S.-T. Pi, S. Y. Savrasov, and W. E. Pickett, Pressure-Tuned Frustration of Magnetic Coupling in Elemental Europium, *Phys. Rev. Lett.* **122**, 057201 (2019).
- [36] V. Pardo and W. E. Pickett, Metal-insulator transition in layered nickelates $\text{La}_3\text{Ni}_2\text{O}_{8-\delta}$ ($\delta = 0.0, 0.5, 1$), *Phys. Rev. B* **83**, 245128 (2011).
- [37] A. S. Botana, V. Pardo, W. E. Pickett, and M. R. Norman, Charge ordering in $\text{Ni}^{1+}/\text{Ni}^{2+}$ nickelates: $\text{La}_4\text{Ni}_3\text{O}_8$ and $\text{La}_3\text{Ni}_2\text{O}_6$, *Phys. Rev. B* **94**, 081105(R) (2016).
- [38] J. Zhang, A. S. Botana, J. W. Freeland, D. Phelan, H. Zheng, V. Pardo, M. R. Norman, and J. F. Mitchell, Mimicking cuprates: large orbital polarization in a metallic square-planar nickelate, *Nat. Phys.* **13**, 864 (2017).
- [39] A. S. Botana, V. Pardo, and M. R. Norman, Electron doped layered nickelates: spanning the phase diagram of the cuprates, *Phys. Rev. Mater.* **1**, 021801 (2017).
- [40] J. Zhang, D. M. Pajerowski, A. S. Botana, H. Zheng, L. Harriger, J. Rodriguez-Rivera, J. P. C. Ruff, N. J. Schreiber, B. Wang, Y.-S. Chen, W. C. Chen, M. R. Norman, S. Rosenkranz, J. F. Mitchell, and D. Phelan, Spin Stripe Order in a Square Planar Trilayer Nickelate, *Phys. Rev. Lett.* **122**, 247201 (2019).
- [41] J. P. Perdew, K. Burke, and M. Ernzerhof, Generalized Gradient Approximation Made Simple, *Phys. Rev. Lett.* **77**, 3865 (1996).
- [42] E. R. Ylvisaker, K. Koepf, and W. E. Pickett, Anisotropy and magnetism in the LSDA+U method, *Phys. Rev. B* **79**, 035103 (2009).
- [43] K. Schwarz and P. Blaha, Solid state calculations using WIEN2k, *Comput. Mater. Sci.* **28**, 259 (2003).
- [44] T. Siegrist, S. M. Zahurak, D. W. Murphy, and R. S. Roth, The parent structure of the layered high-temperature superconductors, *Nature (London)* **334**, 231 (1988).
- [45] K.-W. Lee and W. E. Pickett, Superconductivity in Boron-Doped Diamond, *Phys. Rev. Lett.* **93**, 237003 (2004).
- [46] P. Zhang, S. G. Louie, and M. L. Cohen, Electron-Phonon Renormalization in Cuprate Superconductors, *Phys. Rev. Lett.* **98**, 067005 (2007).
- [47] T. Fukuda, J. Mizuki, K. Ikeuchi, K. Yamada, A. Q. R. Baron, and S. Tsutsui, Doping dependence of softening in the bond-stretching phonon mode of $\text{La}_{2-x}\text{Sr}_x\text{CuO}_4$ ($0 \leq x \leq 0.29$), *Phys. Rev. B* **71**, 060501(R) (2005).
- [48] Y. Quan, S. Ghosh, and W. E. Pickett, Compressed hydrides as metallic hydrogen superconductors, *Phys. Rev. B* **100**, 184505 (2019).